Ultrasonics Sonochemistry 86 (2022) 106007

Contents lists available at ScienceDirect

Ultrasonics Sonochemistry

journal homepage: www.elsevier.com/locate/ultson

Specific chiroptical sensing of cysteine via ultrasound-assisted formation of disulfide bonds in aqueous solution

Jun-Yao Zhang [1], Bei-Bei Yang [1], Ya-Dong Yang, Ru Wang, Li Li [*]

Beijing Key Laboratory of Active Substances Discovery and Druggability Evaluation, Institute of Materia Medica, Chinese Academy of Medical Sciences & Peking Union Medical College, Beijing 100050, China

ARTICLE INFO

Keywords:
Cysteine
Disulfide bond
Chiral sensing
Exciton coupling circular dichroism
Ultrasound

ABSTRACT

Cysteine (Cys) can serve as a biomarker to indicate diseases or disorders, and its chiral sensing has attracted increasing attention. Herein, we established an ultrasound-facilitated chiral sensing method for Cys using 4-chloro-7-nitro-1,2,3-benzoxadiazole (NBD-Cl) and electronic circular dichroism (ECD) spectroscopy. The formation of chiral disulfide bonds induced degenerate exciton coupling between two NBD chromophores, resulting in intense Cotton effects (CEs) of the sensing product. The anisotropy factor (g) was linearly correlated with the enantiomeric excess of Cys across the visible region (400–500 nm), and other natural amino acids or biothiols did not interfere with the detection. This ultrasound-promoted efficient and specific chiral sensing method of Cys has potential for application in the diagnosis of related diseases.

1. Introduction

The dysregulation of L-cysteine (L-Cys) in the brain is related to some neurodegenerative diseases, such as Parkinson's disease and Alzheimer's disease [1–3], whereas D-Cys exerts neuroprotective and therapeutic effects via hydrogen sulfide production from the D-Cys-dependent pathway, which prevents oxidative stress in the brain [4–6]. In recent years, various probes, including molecular sensors [7,8], nanoparticle sensors [9,10], and quantum dot sensors [11], have been developed to recognize Cys enantiomers based on electronic circular dichroism (ECD) or fluorescent response signals.

Ultrasonic waves, which are highly localized and short-lived in liquid medium, can provide abundant energy to generate acoustic cavitation [12–14]. Acoustic cavitation includes the formation, growth, and break-up of bubbles in solution, providing the driving force for manufacturing applications and promoting chemical reactions [15,16]. Benefiting from their environmental-friendliness and sustainability, many ultrasound-assisted methods have been developed for organic synthesis [17–20], especially in the synthesis of various heterocyclic scaffolds [21–23]. Meanwhile, the power and frequency of ultrasound both exert considerable effects on the extent and efficiency of chemical reactions, suggesting that the reaction threshold can be controlled by adjusting the parameters of the apparatus [24,25]. Our previous work showed that ultrasound could decrease the reaction time for chiral sensing [7].

The thiol group endows cysteine with high nucleophilicity and redox susceptibility, thereby facilitating nucleophilic and redox catalysis, allosteric regulation, metal binding, and structural stabilization via the formation or cleavage of disulfide bonds [3,26–31]. Cystine, one of the oxidative products of Cys [32], is hardly soluble in water and is prone to form stones in the kidney [33]. In addition to the chiral carbon centre, disulfide bonds are another intrinsic chiral factor, generating ECD signals at approximately 250 nm [34,35]. The correlations between the chirality of the disulfide bond and the sign of CEs have been studied [36,37]. Sensing Cys by inducing the formation of disulfide bonds may be an efficient method but has seldom been reported.

The construction of products with active ECD signals via molecular probes is an effective and convenient method [7,38,39]. The 7-nitro-1,2,3-benzoxadiazole (NBD) group is electron-deficient and can emit strong fluorescence in typical push–pull systems via photo-induced electron transfer or intramolecular charge transfer pathways [40,41]. Among diverse NBD-based fluorophores, 4-chloro-7-nitro-1,2,3-benzoxadiazole (NBD-Cl, **1**) is frequently used as a fluorescent derivatization

Abbreviations: Cys/C, Cysteine; TEA, triethylamine; A, alanine; R, arginine; N, asparagine; D, aspartic acid; Q, glutamine; E, glutamic acid; G, glycine; H, histidine; I, isoleucine; L, leucine; K, lysine; M, methionine; F, phenylalanine; P, proline; S, serine; T, threonine; W, tryptophan; Y, tyrosine; V, valine; GSH, glutathione; Hcy, homocysteine; L-NAC, N-acetyl-L-cysteine; Pen, penicillamine.

* Corresponding author.
E-mail address: annaleelin@imm.ac.cn (L. Li).

[1] Jun-Yao Zhang and Bei-Bei Yang contributed equally to this work.

https://doi.org/10.1016/j.ultsonch.2022.106007
Received 24 February 2022; Received in revised form 4 April 2022; Accepted 10 April 2022
Available online 14 April 2022

reagent for amino acids, especially for Cys, with high molar extinction coefficients and strong absorption above 300 nm. Due to the higher nucleophilicity of the thiol group than the amino group, derivatization can be achieved more easily. Smiles rearrangement of the NBD group from the thiol group to an amino group subsequently occurs and leaves the thiol free, which means the free thiol group can react again. NBD-Cl (**1**) can distinguish Cys from other amino acids or biothiols in which less active amino group is the only reaction site [42–47]. It is deduced that an efficient exciton coupling will be generated between the NBD groups in the final products and the exciton chirality method (ECM) can be applied [39]. In this study, NBD-Cl was tested for the first time in the chiral sensing of Cys. It was hypothesized that the sensing products could produce UV absorption and ECD responses in the visible region, thus avoiding the interference of other substances. Compared with the N,S-disubstituted product, the product with disulfide bonds was expected to yield more intense CEs due to the degenerate exciton coupling circular dichroism (ECCD) between two NBD chromophores.

Herein, an ultrasound-assisted chiral sensing method for Cys via the construction of disulfide bonds has been developed. The sensing product with a disulfide bond formed quickly and steadily under the synergistic promotion of ultrasound and H_2O_2, giving rise to a perfect bisignate ECCD spectrum. The good linearity and accuracy regarding the enantiomeric composition of Cys are indicated by the anisotropy factor (g factor). Furthermore, other natural amino acids and biothiols were studied for comparison, confirming the selectivity and specificity of this sensing method.

2. Experimental section

2.1. Materials and methods

Reagents and solvents were purchased commercially, and ultrasonic reactions were performed by using a DS-5510DTH ultrasonic cleaner. ECD and UV spectra were recorded on a Jasco J-815 spectrometer (Tokyo, Japan). ^{1}H NMR and ^{13}C NMR spectra were recorded in CD_3OD with a Bruker Avance-600 NMR System. ESI-HRMS data were collected on a Thermo Exactive Orbitrap mass spectrometer.

2.2. Synthesis of sensing products

2.2.1. *Synthesis of N,N-bis(7-nitrobenzo[c][1,2,5]oxadiazol-4-yl) cystine (3)*

L-Cys (30.2 mg, 0.25 mmol) and K_2CO_3 (21.1 mg, 0.15 mmol) were dissolved in 5.5 mL of PBS buffer (pH 7.4, 0.02 mol/L). Then, a solution of compound **1** (49.7 mg, 0.25 mmol) in 1.5 mL of CH_3CN was added. After the addition of 500 μL of an aqueous H_2O_2 solution (0.7 mol/L), the resulting mixture was reacted for 30 min in an ultrasound apparatus (40 kHz, 450 W). The volatiles were removed by rotatory evaporation, and a reddish-brown solid was obtained. The crude product was dissolved in CH_3CN and purified by RP-HPLC to yield compound **3**. ^{1}H NMR (600 MHz, CD_3OD): δ 8.41 (d, J = 8.6 Hz, 1H), 6.36 (d, J = 8.6 Hz, 1H), 3.51 (dd, J = 14.2, 4.9 Hz, 1H), 3.33 (s, 1H), 3.22 (dd, J = 14.1, 8.8 Hz, 1H). ^{13}C NMR (150 MHz, CD_3OD): δ 170.91, 163.00, 144.27, 143.81, 136.21, 123.42, 99.89, 55.56, 39.27. HR-ESIMS: m/z $[M + H]^+$ calcd. for $C_{18}H_{14}N_8O_{10}S_2$ 567.0347, found 567.0326.

2.2.2. *Synthesis of N,S-bis(7-nitrobenzo[c][1,2,5]oxadiazol-4-yl)cysteine (4)*

The same amounts of L-Cys (30.2 mg, 0.25 mmol) and K_2CO_3 (21.1 mg, 0.15 mmol) used in the synthesis of **3** were dissolved in PBS buffer (pH 7.4, 0.02 mol/L) and mixed with a solution of compound **1** (79.4 mg, 0.4 mmol). After ultrasound-promoted reaction for 30 min, compound **4** was prepared using RP-HPLC. ^{1}H NMR (600 MHz, CD_3OD): δ 8.47–8.39 (m, 2H), 7.57 (d, J = 7.8 Hz, 1H), 6.44 (d, J = 8.7 Hz, 1H), 4.24 (dd, J = 14.2, 4.1 Hz, 1H), 3.93 (dd, J = 14.2, 8.7 Hz, 1H), 3.33 (s, 1H). ^{13}C NMR (150 MHz, CD_3OD): δ 170.30, 149.52, 144.31, 143.88, 142.63, 138.00, 136.14, 133.50, 130.82, 124.35, 123.87, 32.86, 29.31. HR-ESIMS: m/z $[M + H]^+$ calcd. for $C_{15}H_9N_7O_8S$ 448.0306, found 448.0289.

2.3. Optimal procedure for the sensing of L-Cys under ultrasonic promotion

A stock solution of **1** (10 mg/mL) was prepared in CH_3CN, and L-Cys was dissolved in water (2 mg/mL) for parallel reactions. To compare the influence of different molar ratios of **1** to L-Cys, gradient molar ratios (0.5, 1, 1.5, 2, 2.5) were employed. The amount of L-Cys (151 μL, 2.5 μmol) was constant, and the added volume of **1** varied from 25 to 125 μL in PBS buffer (pH 7.4, 0.02 mol/L) with a total volume of 2 mL. In addition, multiple reaction conditions were tested, including various solvents, ultrasound powers, and oxidants.

Optimal reaction conditions: aliquots of stock solutions for **1** (50 μL, 2.5 μmol), L-Cys (151 μL, 2.5 μmol), and 0.1 mol/L H_2O_2 (35 μL, 3.5 μmol) were mixed in PBS buffer (pH 7.4, 0.02 mol/L) to a total volume of 2 mL and then placed under ultrasonic conditions (30–45 ℃, 450 W, 40 kHz) for 30 min. The reaction solution was used directly for the measurement of UV and ECD.

The UV and ECD spectra of the reaction solutions were collected with a standard sensitivity of 100 mdeg, a data pitch of 0.5 nm, and a bandwidth of 1 nm; continuous scanning mode was used with a scanning speed of 100 nm/min, a response time of 1 s, and a scanning wavelength range of 350–600 nm using quartz cuvettes with a pathlength of 0.1 cm or 1 cm. The data were baseline-corrected against the corresponding solvent and smoothed using a means-movement equation.

2.4. Fracture and reformulation of disulfide bonds

Tris(2-carboxyethyl)phosphine (TCEP) was dissolved in water to a concentration of 4 mg/mL (0.014 mol/L). A total of 400 μL of reaction solution under the optimal conditions was pipetted in parallel (containing 0.5 μmol of L-Cys) into 4 aliquots and mixed with TCEP at the following molar ratios: (1) 400 μL of reaction solution, (2) 400 μL of reaction solution and 18 μL of TCEP (0.25 μmol), (3) 400 μL of reaction solution and 36 μL of TCEP (0.5 μmol), and (4) 400 μL of reaction solution, 18 μL of TCEP, and 7 μL of 0.1 mol/L H_2O_2 solution (0.7 μmol). Then, these test solutions were diluted to 1 mL with PBS buffer for measurement. ECD and UV spectra were recorded at time points of 5 min, 30 min, 3 h and 24 h.

2.5. Specificity test for Cys against representative amino acids, thiols and Cys derivatives

Solutions (2 mg/mL) of 19 natural L-amino acids, Cys derivatives (L-cysteine ester, L-cystine) and biothiols (L-GSH, L-Hcy, L-NAC, L-Pen) were prepared individually to test the specificity of this sensing method. The same material ratio of the substrate (2.5 μmol), **1** (2.5 μmol) and H_2O_2 (3.5 μmol) was maintained, and the materials were mixed in PBS buffer (pH 7.4, 0.02 mol/L) to a final volume of 2 mL. The aforementioned mixture was reacted for 30 min with the aid of ultrasound from 30 to 45 ℃. There was no ECD signal for other L-amino acids, and only weak CEs were observed for biothiols and derivatives, which were negligible compared with the strong intensity of the sensing products of L-Cys.

2.6. Quantitative test of enantiomeric excess of Cys

According to the optimal reaction conditions described in Section 2.3, three parallel tests were performed with a concentration of 1250 μmol/L. Then, these solutions were diluted with PBS buffer to gradient concentrations (100, 250, 500, 750, 1000, 1250 μmol/L) of Cys. The UV absorbance at 460.5 nm of 3 parallel samples was recorded to obtain average values using a 0.1-cm quartz cuvette. Next, the solutions were

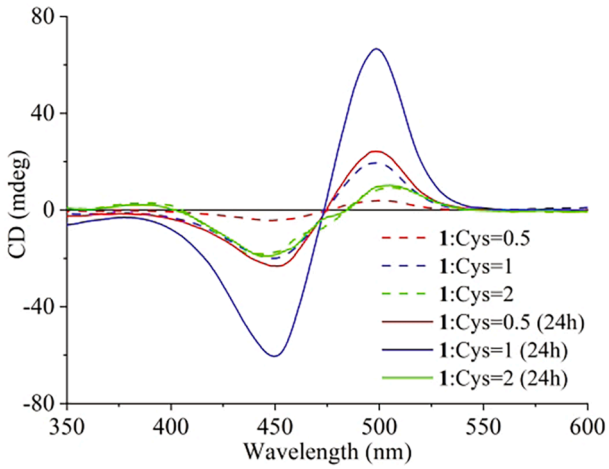

Fig. 1. ECD responses of reaction solutions with different molar ratios of **1** to Cys at different time points (dashed line: instant ECD response; solid line: ECD response after standing for 24 h).

diluted to concentrations of 10, 25, 50, 75, and 100 μmol/L, but the data were recorded in a 1-cm quartz cuvette. Calibration curves were plotted within the two concentration ranges.

D-Cys was dissolved in water at the same concentration as L-Cys (2 mg/mL) and mixed with L-Cys to prepare solutions with different enantiomeric excesses (100%, 80%, 60%, 40%, 20%, 0%, −20%, −40%, −60%, −80%, −100%) with a constant total concentration of 1250 μmol/L. After ultrasonic promotion for 30 min, these reaction solutions were directly used for ECD analysis. The g-factors ($g = \theta/(32980 \times A)$, θ: ECD data, A: UV absorbance) at 498 and 448 nm were plotted against the enantiomeric excess of Cys to generate calibration curves. The spectroscopic measurements were carried out at least three times, and average values were used.

2.7. Application of a calibration curve to calculate enantiomeric excess

Ten aliquots of solution with different enantiomeric excesses (70%, 50%, 25%, 10%, 5%, −5%, −25%, −50%, −70%) were reacted according the procedure described above. These samples were diluted to different concentrations, and the g-factors of CE at 498 and 448 nm were utilized to calculate the enantiomeric excess according to the calibration curves established above.

2.8. Computation details

Quantum-chemical calculation procedures for compounds **3** and **4** were established as follows: First, molecular dynamics analysis was performed via XTB software [48], and 2000 conformations were generated for each compound in 100 ps. Then, the Molclus package [49] was utilized to sort these conformations into clusters. The results were submitted to XTB, and initial optimizations in gas and water were performed. After ranking those conformations, 10, 12, and 12 conformers populated more than 0.1% for compound **3** with *P*-disulfide bond ((*P*)-**3**), **3** with *M*-disulfide bond (*M*)-**3**, and **4**, respectively, were chosen for density-functional theory (DFT) and its time-dependent variant (TDDFT) calculations using Gaussian16 Rev B.01 [50]. B3LYP with dispersion correction (B3LYP-D3) and the 6-311G(d,p) basis set were used, and the lowest 100 electronic transitions were set. A solvation model based on density (SMD) was adopted to simulate the solvent effects. Finally, based on the Gibbs free energies calculated under conditions of 298.15 K and 1 atm pressure, the most populated conformers were identified. The Boltzmann-averaged ECD spectra were obtained with σ as 0.25 eV by SpecDis1.71 software [51].

3. Results and discussion

3.1. Optimization of the sensing process

3.1.1. Influence of the molar ratio of *1* to Cys

For N-arylation derivatization of common amino acids, excess NBD analogues and harsh conditions, such as prolonged stirring with heating, are needed to achieve a high yield [52–55]. However, for Cys, the thiol group is more nucleophilic than amino group. After reacting with the chlorine atom of **1**, Smiles rearrangement occurs [42–47] to transfer the NBD group from thiol group to amino group. Thus, the energy barrier for N-arylation is greatly decreased, and the free thiol group can be oxidized [56,57].

Here, experiments with different molar ratios of **1** (0.5, 1, 1.5, 2, 2.5) to L-Cys were carried out with ultrasound (360 W, 40 kHz) for 30 min in PBS buffer (pH 7.4, 0.02 mol/L), and molar ratios of 0.5, 1, and 2 were selected for further discussion. The instant response at a molar ratio of 1 was much stronger than the responses at molar ratios of 0.5 and 2 (Fig. 1). After 24 h, the CE intensity of the samples with molar ratios of 1 and 0.5 increased substantially, but that of the sample with a molar ratio of 2 remained unchanged (Fig. 1).

The interconversions of sensing products took place, as determined by HPLC (Fig. S1), confirming the rearrangement of NBD from a thiol

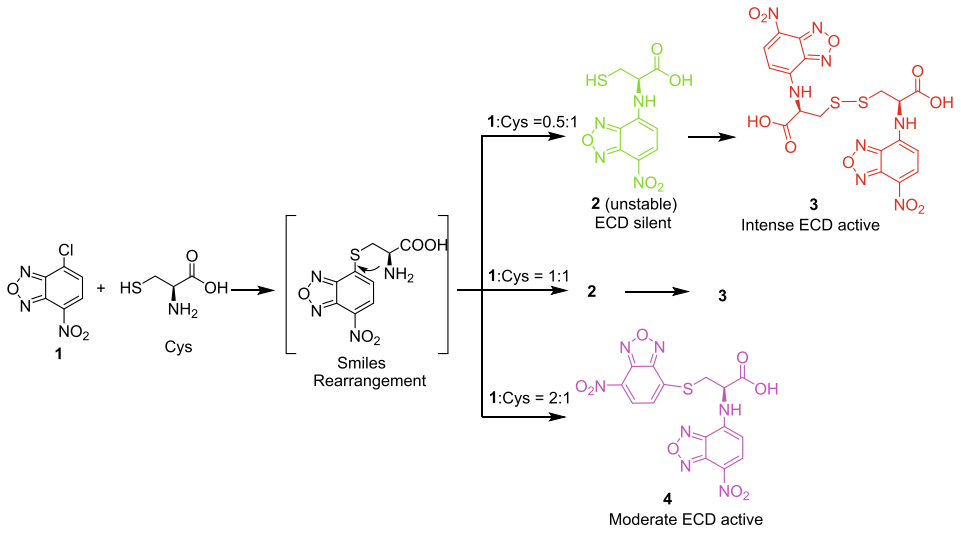

Scheme 1. Reactions between NBD-Cl (**1**) and Cys at different molar ratios.

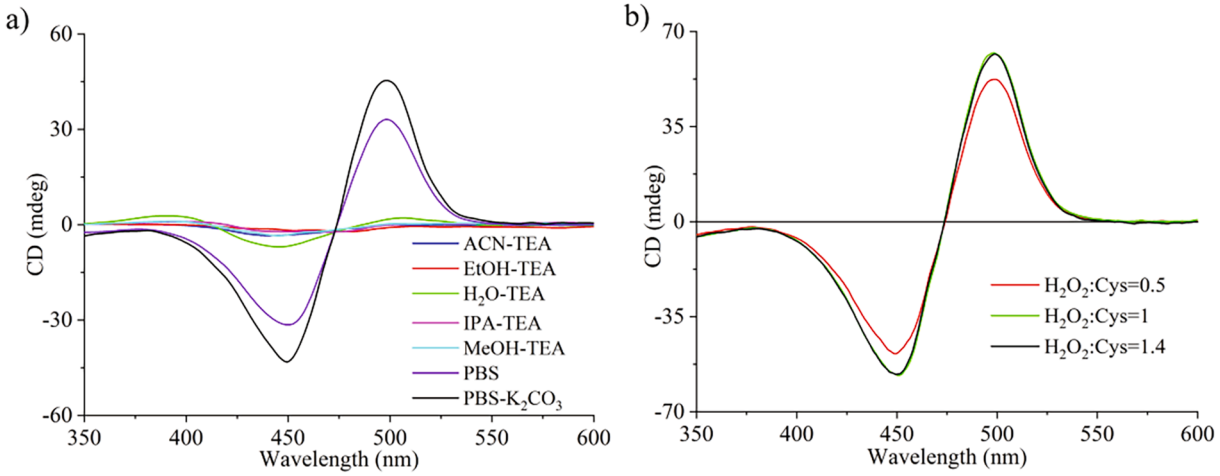

Fig. 2. ECD responses of reaction solutions in different media. a) Different solvents; b) the addition of H_2O_2 (0.1 mol/L) at different molar ratios.

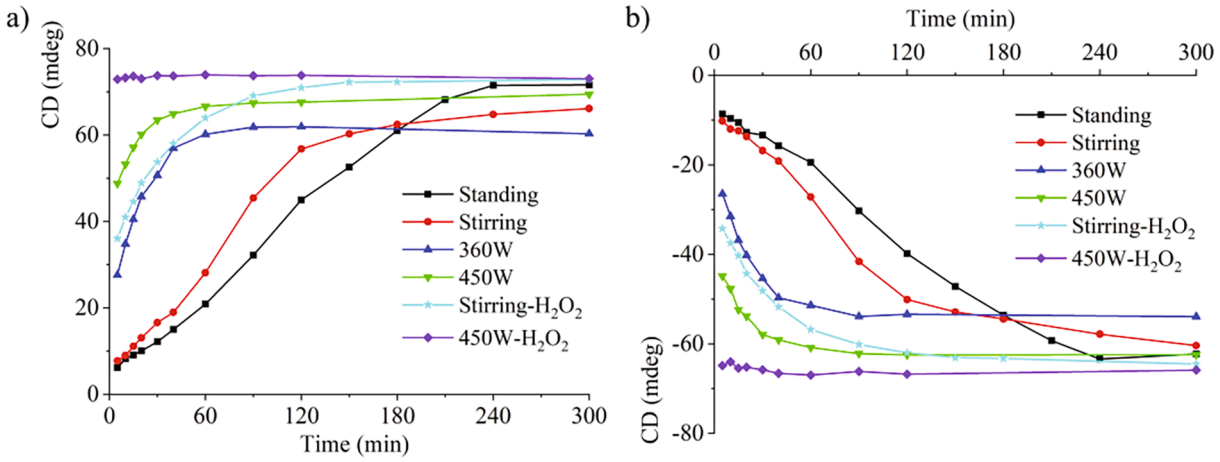

Fig. 3. Correlation of the reaction over time under different conditions. a) Monitored CD responses at 498 nm; b) monitored CD responses at 448 nm.

group to an amino group (Scheme 1). The free thiol group of **2** is liable to dimerize or react with another NBD-Cl molecule, accounting for its instability. Thus, the instant products of **1** and Cys at a molar ratio of 0.5:1 or 1:1 were complex. Herein, as NBD-Cl was used up and compound **2** remained, final product **3** with a disulfide bond was formed via slow spontaneous oxidation. Moreover, when sensor **1** was in excess in solution, the thiol group could substitute the chlorine atom on **1** without oxidation. Thus, the sensing product at a molar ratio of 2:1 was compound **4**, which remained unchanged over time. This result indicated that compound **3** with a disulfide bond could not be formed unless the thiol group was free. Excess sensor **1** underwent N,S-diarylation and prevented the formation of disulfide bonds. The structures of compounds **3** and **4** were confirmed by NMR and HR-ESIMS (Figs. S2–S7).

3.1.2. Optimization of the sensing conditions

The sensing reaction was evaluated in six commonly used solvents: methanol (MeOH), ethanol (EtOH), isopropanol (IPA), acetonitrile (ACN), deionized water (H_2O) and PBS buffer (pH 7.4, 0.02 mol/L). When reactions were conducted in neutral or acidic medium, there were only negligible ECD signals for those solutions (Fig. S8). With different optimizations, it was shown that the solvent and the base exerted great effects on the reaction process. Intense bisignate ECCD appeared in PBS buffer, and the addition of K_2CO_3 promoted the reaction more effectively than triethylamine (TEA) (Fig. 2a).

Hydrogen peroxide (H_2O_2) is an effective environmentally friendly oxidant that can significantly promote the sensing process. The strongest ECD signal appeared when the molar ratio of H_2O_2 (0.1 mol/L) to Cys was greater than 1 (Fig. 2b). In contrast to harsh conditions for **1** to derive amino acids other than Cys [52–55], the optimized reaction conditions were mild.

3.1.3. Promotion by ultrasound

In the chemical structure of **1**, the lone pair on the chlorine atom is involved in resonance with the benzene ring to create a double bond and it is tough for the thiol group to replace the chlorine atom without any catalysis. Here, ultrasound exerted considerable effects on the extent and efficiency of the sensing reaction. It can produce many cavitations in solutions to facilitate reactants being well mixed and exposed to oxygen in air more sufficiently. In addition, it provided abundant energy for the reaction to overcome the energy barrier more easily. After 30 min of reaction, the CE intensities at 498 nm and 448 nm of the reaction mixtures were plotted against time under various conditions. As shown in Fig. 3, ultrasound promotion generated more intense CD signals than stirring promotion and shortened the time to reach the equilibrium. The CE intensity obtained with 450-W promotion was higher than that obtained with the 360-W promotion, indicating that the ultrasound power exerted great effects on the reaction equilibrium.

With the addition of H_2O_2, the instantaneous CD values increased when the reaction was ended. Ultrasound (450 W, 40 kHz) with the addition of dilute H_2O_2 solution (0.1 mol/L) led to a complete reaction. The CE intensity reached a maximum value after the 30-min reaction and remained nearly unchanged for the next 5 h (Fig. 3 and Fig. S9). This

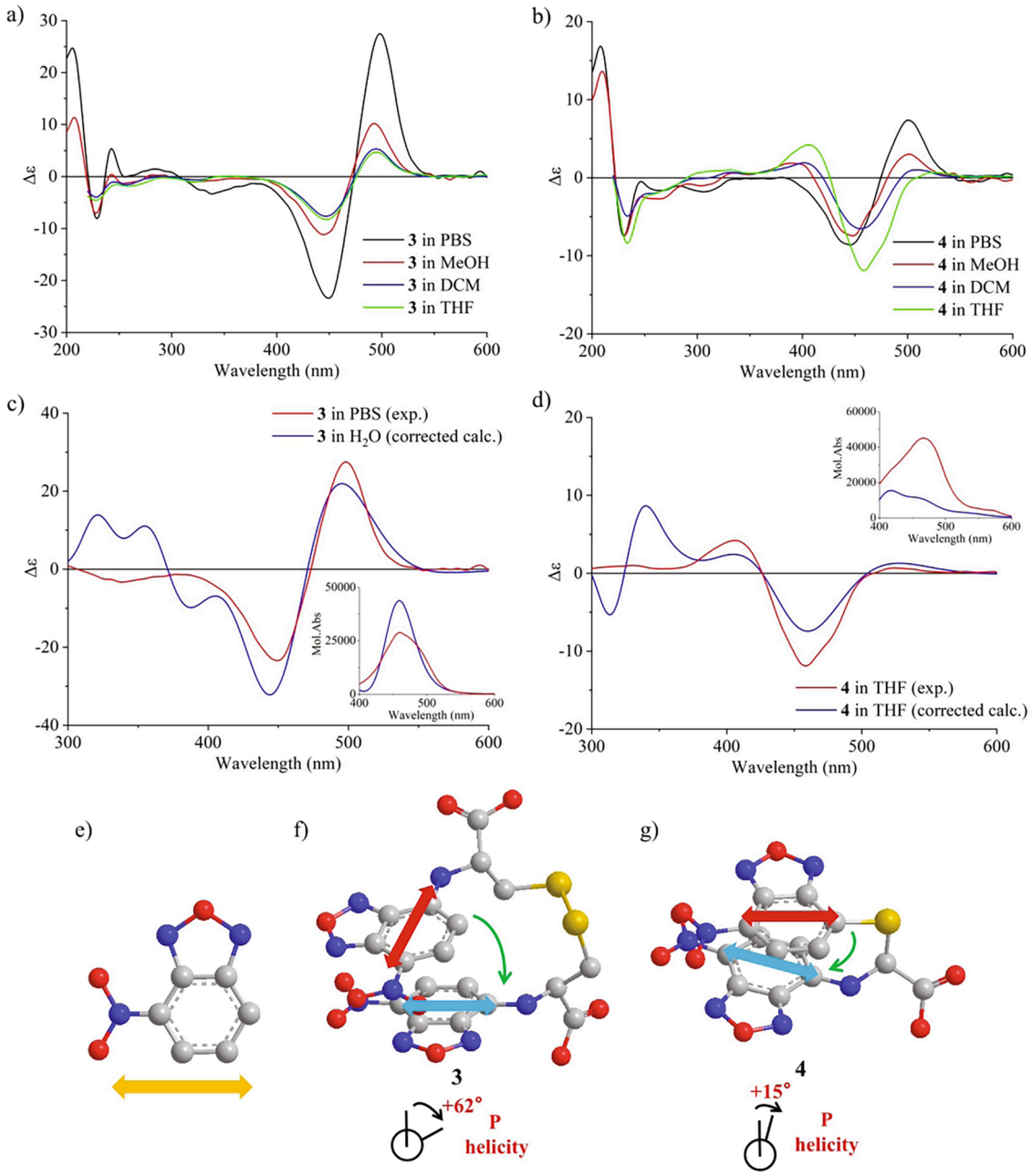

Fig. 4. Comparison of the ECD curves for **3** and **4** in different solvents and information about the transition of excited states. a) Experimental ECD curves of **3** in different solvents; b) experimental ECD curves of **4** in different solvents; c) comparison of experimental and corrected calculated (40-nm redshift) ECD curves of **3** (B3LYP/6-311G(d,p), SMD/water), inset: experimental and corrected calculated UV curves of **3** at 400–600 nm; d) comparison of experimental and corrected calculated (15-nm redshift) ECD curves of **4** (B3LYP/6-311G(d,p), SMD/THF), inset: experimental and corrected calculated UV curves of **4** at 400–600 nm; e) transition dipole moment of NBD group; f) helicity of transition dipole moments for **3** (B3LYP-D3/6-311G(d,p), SMD/water); g) helicity of transition dipole moments for **4** (B3LYP-D3/6-311G(d,p), SMD/THF).

fact demonstrated that the change in ECD signals was related to the oxidation process, as both ultrasound and H_2O_2 facilitated the formation of disulfide bonds, which thus greatly promoted sensing.

3.2. *ECD spectra of sensing products **3** and **4***

Bisignate CEs exist at approximately 400 to 500 nm for **3** and **4** (Fig. 4a-4b). The spectra of **3** can be divided into two characteristic regions, 200–300 nm and 300–600 nm, especially in PBS buffer, which were attributed to the contribution of disulfide bonds and electronic transitions from NBD chromophores, respectively. For **4**, only the transition dipole moments of two NBD groups mattered.

3.2.1. *Helicity of disulfide bond*

The disulfide bond is an inherently asymmetrical chromophore, and the sign of its first CE was correlated with the dihedral angle of C-S-S-C [36,37] (Fig. S10). The normal disulfide dihedral angle was deduced to be near 90° [57,58]. In the presence of extra chiral centres, preferences for *M* (left-handed) or *P* (right-handed) helicity might both exist. For compound **3**, a positive CE appeared at 250 nm in PBS and methanol (Fig. 4a). According to the quadrant rule for the inherent optical activity of disulfides, the dihedral angle was supposed to be in the region of 0°~90° (*P*) or −180°~−90° (*M*) (Fig. S10).

To test this assumption, geometry optimization and electronic transition calculations were carried out for (*P*)-**3** and (*M*)-**3**, with the

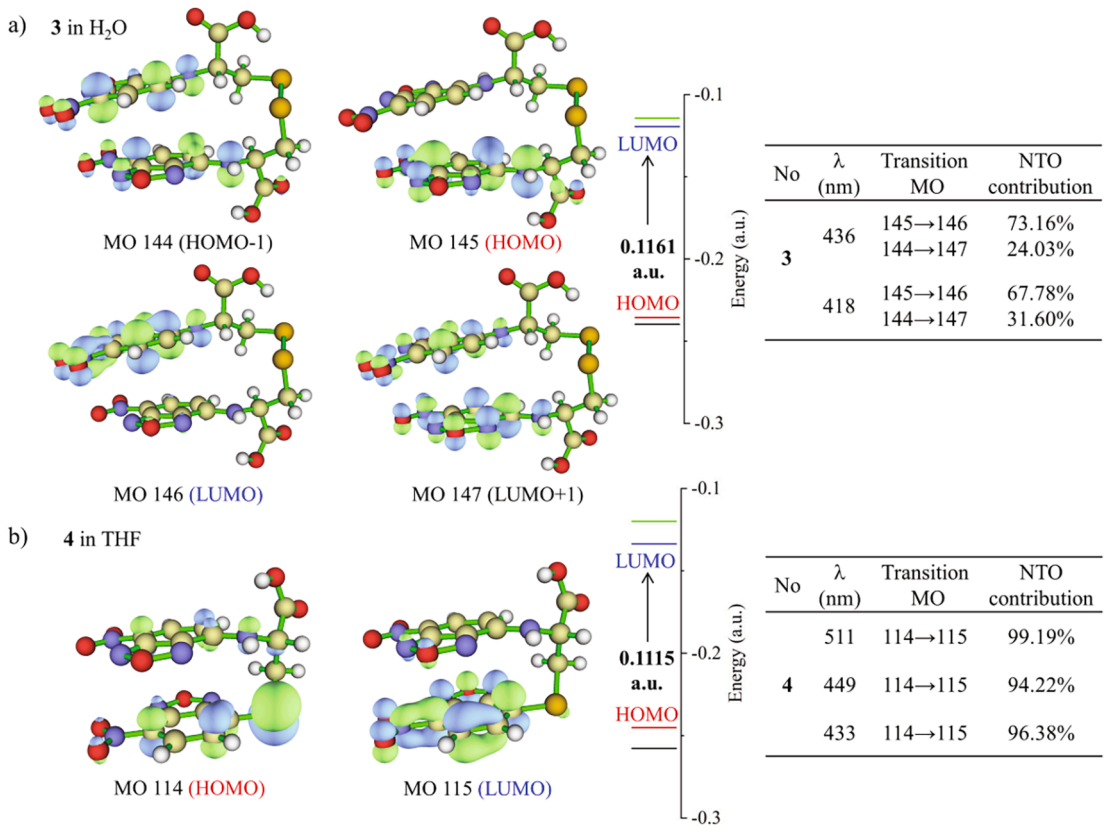

No	λ (nm)	Transition MO	NTO contribution
3	436	145→146	73.16%
		144→147	24.03%
	418	145→146	67.78%
		144→147	31.60%

No	λ (nm)	Transition MO	NTO contribution
4	511	114→115	99.19%
	449	114→115	94.22%
	433	114→115	96.38%

Fig. 5. NTO analysis in the transition of electronic states for (*P*)-**3** and **4**. a) Molecular orbitals (MOs) involved for **3** in H_2O and their contributions to NTOs with the diagram of energy levels (B3LYP-D3/6-311G(d,p), SMD/water); b) MOs involved for **4** in THF and their contributions to NTOs with the diagram of energy levels (B3LYP-D3/6-311G(d,p), SMD/THF).

disulfide bonds being *P* and *M* configurations, respectively. In agreement with the estimation, the calculated ECD spectra both displayed a positive CE in absorption region of disulfide bond. Furthermore, the Gibbs free energy of the lowest-energy conformer of (*P*)-**3** was much lower (ΔG = −426.4 kJ/mol) than that of (*M*)-**3**. Thus, the disulfide bond with P helicity was adopted for subsequent ECD interpretation.

3.2.2. *ECM between NBD groups*

The experimental ECD spectra of **3** and **4** differed tremendously in terms of the shape and intensity at 400–500 nm (Fig. 4a-4b), which was ascribed to different interactions between the NBD chromophores.

An intense bisignate exciton couplet appeared at 400–500 nm in the experimental ECD spectra of **3** (Fig. 4c), which was ascribed to degenerate exciton coupling (DEC) between two identical NBD-NH-R groups. The CE intensity varied with the polarity of the solvent, and less polar solvents (DCM and THF) yielded the weakest CE signals. However, for compound **4**, the intensity of the positive CE at approximately 500 nm was much weaker than that of the negative CE at 448 nm (Fig. 4d). This could be attributed to the nondegenerate exciton coupling (NDEC) between the NBD-NH-R and NBD-S-R groups (Fig. 4e). As three prerequisites for the application of ECM were satisfied, the helicity of transition dipole moments between NBD-R groups resulted in an ECCD spectrum with two bisignate CEs (Fig. 4e-4g) [39,59,60]. According to the positive CE at longer wavelengths (498 nm), a clockwise screw of two transition dipole moments was deduced (Fig. 4f-4g).

The ECD spectra of **3** and **4** were further investigated using DFT and TDDFT calculations. Based on the B3LYP-D3/6-311G(d,p) geometries, various hybrid functionals together with 6-311G(d,p) or TZVP basis set were used to reproduce the experimental ECD spectra for compound **3** in H_2O, including B3LYP, Cam-B3LYP, PBE1PBE, M06-2X and ωB97XD. All the calculations offered a bisignate CE at the long wavelength with different deviations from the experimental counterpart (Fig. S11). Therein, the calculated ECD spectrum for (*P*)-**3** using the B3LYP/6-311G(d,p) approach was the most consistent with the experimental spectrum after a 40-nm redshift. For the ECD spectrum of compound **4** in THF, the shape of the bisignate CE at 400–500 nm was greatly different from that in PBS, and thus it was selected for further analysis. Calculation results after a 15-nm redshift indicated that the observed couplet of **4** was actually two isolated ECD bands. The two CE bands corresponded to the UV maximum for the NBD-S-R and NBD-NH-R groups, which was the characteristic of NDEC. These two UV peaks were merged to form a broad peak in the experimental spectra.

Herein, natural transition orbitals (NTOs) were applied to analyse the transitions of electronic states. In this way, only one or few orbital pairs can play dominant roles in electron excitation, which eliminates the interferences from other molecular orbitals (MOs) [61,62]. For compound **3**, the excitations at 436 and 418 nm contributed to the positive and negative CE bands in the theoretical ECD spectrum, which corresponded to the couplet at 498 and 448 nm. Two occupied (HOMO-1 and HOMO) and two unoccupied MOs (LUMO and LUMO + 1) constitute NTO pairs with the highest eigenvalues in this degenerate exciton coupling and yield the split ECD (Fig. 5a). In contrast, for **4** in THF, the electronic transition from the occupied MO (HOMO) to the unoccupied MO (LUMO) contributes mostly to CEs in the visible region (Fig. 5b). Moreover, the first positive CE became weaker with the decrease in solvent polarity, which might be ascribed to the small angle between the transition dipole moments of the NBD-S-R and NBD-NH-R groups.

The UV–Vis spectra can be converted to Tauc plots whose X-axis intercept of the tangent line can be used to predict the energy gap (E_g) [63,64]. Here, it was supposed that **3** and **4** had a direct band gap to check whether $(\alpha h\nu)^2$ showed any linear part against energy ($E = h\nu$)

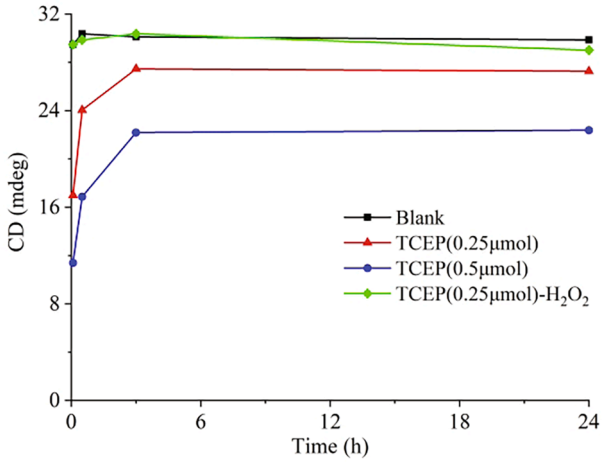

Fig. 6. ECD responses of 30-min reaction solutions with different molar ratios of TCEP to disulfide bond versus time (h) at 498 nm.

[63]. Otherwise, equations for indirect band gap need be used. In the region of 2–3 eV, there were perfect linear parts in the Tauc plots of **3** and **4**, and the E_g was extrapolated as 2.45 eV and 2.41 eV, respectively (Fig. S12). In TDDFT analysis, the energy gaps between the HOMO and LUMO were 3.16 eV and 3.03 eV, respectively. The difference between the theoretical and experimental energy gaps was related to the absorption wavelength and confirmed the necessity of redshift for the calculated spectra.

3.3. Verification of the disulfide bonds by ECD spectroscopy

TCEP is widely used as a quantitative reducing agent of disulfide bonds in protein chemistry and proteomics [65]. The reduction of disulfide bonds by TCEP can be completed in less than 5 min at room temperature.

The reaction solution under optimal conditions was diluted to 500 μmol/L for 4 aliquots. The first one was used as a blank solution, while the second and the third aliquots were used to test the influence of different ratios of TCEP relative to the disulfide bond. For the last aliquot, TCEP was added, and then H_2O_2 was added. Five minutes, 30 min, 3 h, and 24 h were set as sampling points to record CD signals at 498 nm after the 30-min sensing reaction. It was demonstrated that the addition of TCEP decreased the ECD signals and that excess TCEP exerted more effects. Furthermore, H_2O_2 will destroy the reducibility of TCEP as a high similarity between the blank and the solution with both H_2O_2 and TCEP was observed (Fig. S13). Later, the disrupted disulfide bond can be partially formed in autoxidation, but it cannot recover to the original intensity (Fig. 6). It also confirmed that the intense intensity was related to the existence of disulfide bonds and that disulfide bonds

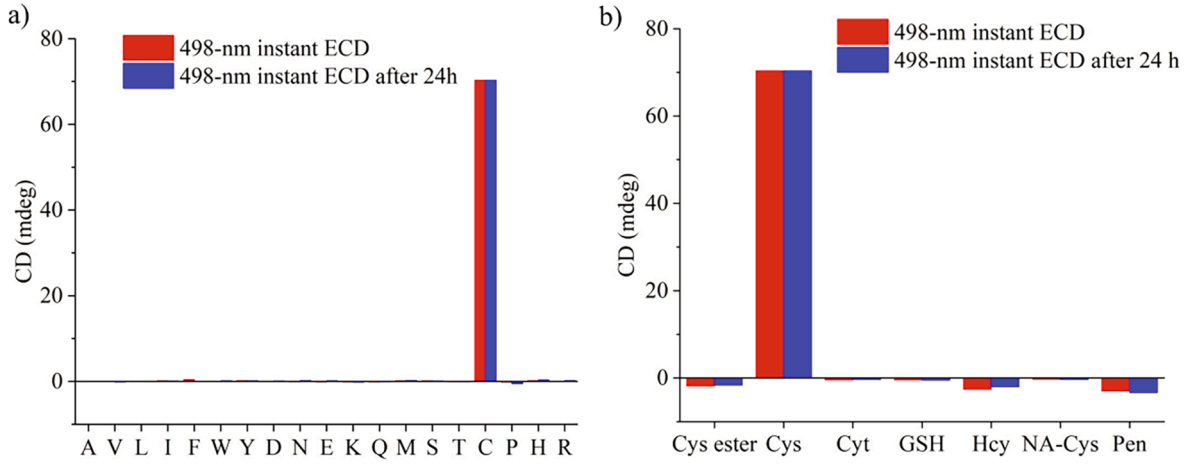

Fig. 7. The 498-nm ECD responses of 30-min reaction solutions for different substrates. a) 498-nm ECD responses for amino acids; b) 498-nm ECD responses for biothiols and cysteine derivatives.

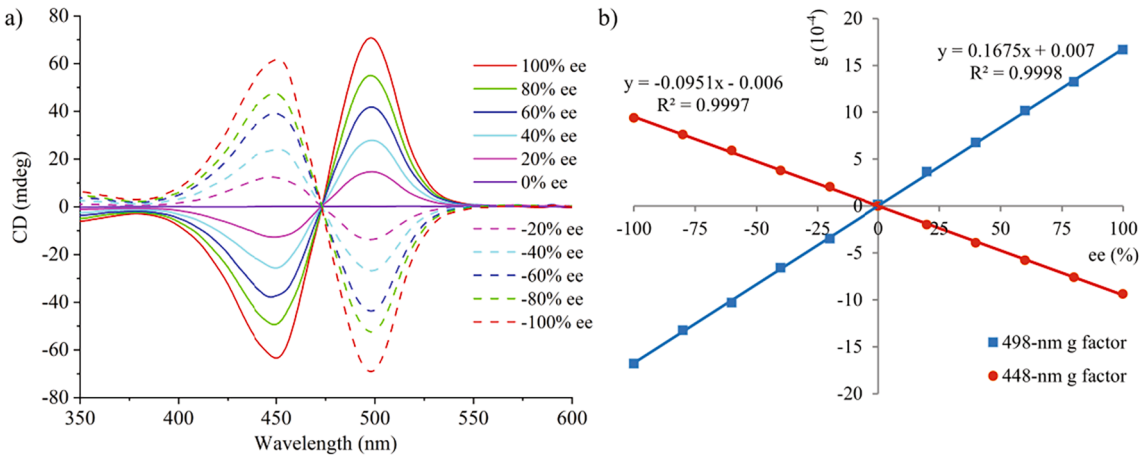

Fig. 8. ECD spectra and calibration curves of ee for Cys solution. a) ECD spectra of Cys solution with different ee values; b) the calibration curves between the g factor at 498 nm/448 nm and ee of the Cys solution.

Table 1
Chiral sensing results for Cys by **1**.

Sample composition ee (%)	Sensing results of Cys solutions			
	ee (498 nm, %)	ee (448 nm, %)	Average (%)	Error (%)
70	72.26	68.88	70.57	0.43
50	49.77	48.71	49.24	−0.76
25	25.62	23.48	24.55	−0.45
10	10.24	9.40	9.82	−0.18
5	4.79	5.39	5.09	0.09
−5	−4.92	−5.28	−5.10	−0.10
−10	−9.21	−10.49	−9.85	0.39
−25	−25.35	−25.89	−25.62	−0.62
−50	−48.74	−50.29	−49.52	0.48
−70	−70.96	−70.99	−70.98	−0.98

can form spontaneously in the presence of naked thiol groups.

3.4. Specificity against other amino acids, thiols and Cys derivatives

Natural L-amino acids and common biothiols or cysteine derivatives were investigated to evaluate the specificity of the method. This method showed a high specificity for Cys due to the formation of disulfide bonds. Under the optimal reaction conditions, no obvious ECD signals were observed for the other 18 amino acids immediately or after 24 h (Fig. 7a).

Regarding biothiols and cysteine derivatives, only weak CEs were observed in the ECD spectra of L-Pen, Hcy and cystine (Cys-Cys). No increase in the signal intensity was observed after 24 h of incubation in the solutions (Fig. 7b). Although the sensing product of cystine was deduced to possess the same skeleton as **3**, its weak ECD signals indicated the low reactivity of the amino group with sensor **1**. This fact also suggested that Smiles rearrangement from thiol arylation to amino arylation greatly facilitated the sensing of Cys.

3.5. Quantitative sensing for enantiomeric excess of Cys

Quantitative sensing of Cys in terms of enantiomeric excess was analysed by ECD and UV spectroscopy. The UV absorbance at 460.5 nm increased linearly within two concentration ranges (10–100 μmol/L, 100–1250 μmol/L) of L-Cys when using cuvettes with different pathlengths (1 cm/0.1 cm) (Fig. S14). The sensitivity of most Cys chiral sensing methods is at the micromolar level [7–11]. In addition, it has been reported that the concentration of Cys in healthy bodies ranges from 15 to 30 μm and elevated levels may indicate disorders in the brain or kidney [1–3]. Thus, the quantitation limit of 10 μmol/L is sufficient for biosensing of chiral Cys.

The anisotropy factor (g factor) was used to assess the enantiomeric excess (ee), avoiding the influence of concentration fluctuation. Good linear correlations were obtained between g-factors at 498 and 448 nm against ee from −100% to 100% of Cys at a concentration of 1250 μmol/L (Fig. 8).

To test the accuracy of the two regression equations, ten samples of chiral Cys were prepared with different enantiomeric excesses at various concentrations. The average detection errors at two wavelengths were no more than 1.0% (Table 1), implying the potential for high-throughput screening applications [66].

4. Conclusions

In this work, an ultrasound-promoted chiral sensing approach for Cys was developed by increasing the ECD signal through the formation of disulfide bonds. This method displayed intense enantioselective ECD signals over 350 nm without interference from reagents. The g factors at 498 nm and 448 nm were used to accurately determine the enantiomeric excess of Cys. Due to the nucleophilicity of the thiol group and Smiles rearrangement of the NBD group, high sensitivity and selectivity towards Cys against other natural amino acids and biothiols were observed. The maximum measurement error was approximately 1%, which is reliable for high-throughput screening, proving the potential of ultrasound to promote the formation of disulfide bonds for Cys and the employment of disulfide bonds in the sensing field.

Notes

The authors declare no competing financial interest.

CRediT authorship contribution statement

Jun-Yao Zhang: Methodology, Investigation, Writing – original draft. **Bei-Bei Yang:** Conceptualization, Validation. **Ya-Dong Yang:** Data curation, Formal analysis. **Ru Wang:** Resources. **Li Li:** Conceptualization, Supervision, Writing – review & editing.

Declaration of Competing Interest

The authors declare that they have no known competing financial interests or personal relationships that could have appeared to influence the work reported in this paper.

Acknowledgements

This work was financially supported by the CAMS Innovation Fund for Medical Sciences (CIFMS, No. 2016-I2M-3-009).

Appendix A. Supplementary data

Supplementary data to this article can be found online at https://doi.org/10.1016/j.ultsonch.2022.106007.

References

[1] B.D. Paul, J.I. Sbodio, S.H. Snyder, Cysteine metabolism in neuronal redox homeostasis, Trends Pharmacol. Sci. 39 (2018) 513–524, https://doi.org/10.1016/j.tips.2018.02.007.
[2] D. Petrovic, E. Kouroussis, T. Vignane, M.R. Filipovic, The role of protein persulfidation in brain aging and neurodegeneration, Front. Aging Neurosci. 13 (2021) 320, https://doi.org/10.3389/fnagi.2021.674135.
[3] C. Valle, M.T. Carrì, Cysteine modifications in the pathogenesis of ALS, Front. Mol. Neurosci. 10 (2017) 5, https://doi.org/10.3389/fnmol.2017.00005.
[4] T. Seki, M. Sato, A. Konno, H. Hirai, Y. Kurauchi, A. Hisatsune, H. Katsuki, D-Cysteine promotes dendritic development in primary cultured cerebellar Purkinje cells via hydrogen sulfide production, Mol. Cell. Neurosci. 93 (2018) 36–47, https://doi.org/10.1016/j.mcn.2018.10.002.
[5] N. Shibuya, S. Koike, M. Tanaka, M. Ishigami-Yuasa, Y. Kimura, Y. Ogasawara, K. Fukui, N. Nagahara, H. Kimura, A novel pathway for the production of hydrogen sulfide from D-cysteine in mammalian cells, Nat. Commun. 4 (2013) 1366, https://doi.org/10.1038/ncomms2371.
[6] T. Ohta, Y. Morikawa, M. Sato, A. Konno, H. Hirai, Y. Kurauchi, A. Hisatsune, H. Katsuki, T. Seki, Therapeutic potential of D-cysteine against in vitro and in vivo models of Spinocerebellar ataxia, Exp. Neurol. 343 (2021), 113791, https://doi.org/10.1016/j.expneurol.2021.113791.
[7] F. Xiong, J.-Y. Zhang, T.-T. Du, B.-B. Yang, X.-G. Chen, L. Li, Ultrasound-promoted specific chiroptical sensing of cysteine in aqueous solution and cells, Microchem. J. 153 (2020) 104471, https://doi.org/10.1016/j.microc.2019.104471.
[8] F.Y. Thanzeel, C. Wolf, Substrate-specific amino acid sensing using a molecular D/L-cysteine probe for comprehensive stereochemical analysis in aqueous solution, Angew. Chem. Int. Ed. 56 (2017) 7276–7281, https://doi.org/10.1002/anie.201701188.
[9] J. Wang, X. Xu, X. Qiu, S. Zhang, Y. Peng, Yolk–shell structured Au@Ag@mSiO$_2$ as a probe for sensing cysteine enantiomers and Cu^{2+} based on circular dichroism, Analyst 144 (2019) 7489–7497, https://doi.org/10.1039/C9AN01541H.
[10] F. Zhu, X. Li, Y. Li, M. Yan, S. Liu, Enantioselective circular dichroism sensing of cysteine and glutathione with gold nanorods, Anal. Chem. 87 (2015) 357–361, https://doi.org/10.1021/ac504017f.
[11] F. Ghasemi, M.R. Hormozi-Nezhad, M. Mahmoudi, Time-resolved visual chiral discrimination of cysteine using unmodified CdTe quantum dots, Sci. Rep. 7 (2017) 890, https://doi.org/10.1038/s41598-017-00983-2.
[12] T.G. McKenzie, F. Karimi, M. Ashokkumar, G.G. Qiao, Ultrasound and sonochemistry for radical polymerization: sound synthesis, Chem. Eur. J. 25 (2019) 5372–5388, https://doi.org/10.1002/chem.201803771.

[13] P.N. Amaniampong, F. Jérôme, Catalysis under ultrasonic irradiation: a sound synergy, Curr. Opin. Green Sust. 22 (2020) 7–12, https://doi.org/10.1016/j.cogsc.2019.11.002.
[14] S.K. Bhangu, M. Ashokkumar, Theory of sonochemistry, in: J.C. Colmenares, G. Chatel (Eds.), Sonochemistry: From Basic Principles to Innovative Applications, Springer International Publishing, Cham, 2017, https://doi.org/10.1007/978-3-319-54271-3_1.
[15] W. Bonrath, Ultrasound supported catalysis, Ultrason. Sonochem. 12 (2005) 103–106, https://doi.org/10.1016/j.ultsonch.2004.03.008.
[16] H. Xu, B.W. Zeiger, K.S. Suslick, Sonochemical synthesis of nanomaterials, Chem. Soc. Rev. 42 (2013) 2555–2567, https://doi.org/10.1039/C2CS35282F.
[17] B. Banerjee, Recent developments on ultrasound assisted catalyst-free organic synthesis, Ultrason. Sonochem. 35 (2017) 1–14, https://doi.org/10.1016/j.ultsonch.2016.09.023.
[18] B. Banerjee, Recent developments on ultrasound-assisted organic synthesis in aqueous medium, J. Serb. Chem. Soc. 82 (2017) 755–790, https://doi.org/10.2298/JSC170217057B.
[19] B. Banerjee, Ultrasound and nano-catalysts: an ideal and sustainable combination to carry out diverse organic transformations, ChemistrySelect 4 (2019) 2484–2500, https://doi.org/10.1002/slct.201803081.
[20] G. Kaur, A. Sharma, B. Banerjee, Ultrasound and ionic liquid: an ideal combination for organic transformations, ChemistrySelect 3 (2018) 5283–5295, https://doi.org/10.1002/slct.201800326.
[21] B. Banerjee, Recent developments on ultrasound-assisted one-pot multicomponent synthesis of biologically relevant heterocycles, Ultrason. Sonochem. 35 (2017) 15–35, https://doi.org/10.1016/j.ultsonch.2016.10.010.
[22] B. Banerjee, Recent developments on ultrasound-assisted synthesis of bioactive N-heterocycles at ambient temperature, Aust. J. Chem. 70 (2017) 872–888, https://doi.org/10.1071/CH17080.
[23] A. Sharma, A. Priya, M. Kaur, A. Singh, G. Kaur, B. Banerjee, Ultrasound-assisted synthesis of bioactive S-heterocycles, Synth. Commun. 51 (2021) 3209–3236, https://doi.org/10.1080/00397911.2021.1970775.
[24] A. Brotchie, F. Grieser, M. Ashokkumar, Effect of power and frequency on bubble-size distributions in acoustic cavitation, Phys. Rev. Lett. 102 (2009), https://doi.org/10.1103/PhysRevLett.102.084302, 084302.
[25] R.J. Wood, J. Lee, M.J. Bussemaker, A parametric review of sonochemistry: control and augmentation of sonochemical activity in aqueous solutions, Ultrason. Sonochem. 38 (2017) 351–370, https://doi.org/10.1016/j.ultsonch.2017.03.030.
[26] N.J. Pace, E. Weerapana, Diverse functional roles of reactive cysteines, ACS Chem. Biol. 8 (2013) 283–296, https://doi.org/10.1021/cb3005269.
[27] L.B. Poole, The basics of thiols and cysteines in redox biology and chemistry, Free Radic. Biol. Med. 80 (2015) 148–157, https://doi.org/10.1016/j.freeradbiomed.2014.11.013.
[28] C.E. Paulsen, K.S. Carroll, Cysteine-mediated redox signaling: chemistry, biology, and tools for discovery, Chem. Rev. 113 (2013) 4633–4679, https://doi.org/10.1021/cr300163e.
[29] P.J. Hogg, Disulfide bonds as switches for protein function, Trends Biochem. Sci. 28 (2003) 210–214, https://doi.org/10.1016/S0968-0004(03)00057-4.
[30] A. Manteca, Á. Alonso-Caballero, M. Fertin, S. Poly, D. De Sancho, R. Perez-Jimenez, The influence of disulfide bonds on the mechanical stability of proteins is context dependent, J. Biol. Chem. 292 (2017) 13374–13380, https://doi.org/10.1074/jbc.M117.784934.
[31] M. Góngora-Benítez, J. Tulla-Puche, F. Albericio, Multifaceted roles of disulfide bonds. peptides as therapeutics, Chem. Rev. 114 (2014) 901–926, https://doi.org/10.1021/cr400031z.
[32] X. Zhang, B. Yang, W. Zhou, Z. Zhu, Y. Bian, R. Zeng, Dynamic detection of thiol oxidation/reduction status during the conversion of cysteine/cystine, J. Mol. Struct. 1250 (2022) 131675, https://doi.org/10.1016/j.molstruc.2021.131675.
[33] D. Rimer Jeffrey, Z. An, Z. Zhu, H. Lee Michael, S. Goldfarb David, A. Wesson Jeffrey, D. Ward Michael, Crystal growth inhibitors for the prevention of L-cystine kidney stones through molecular design, Science 330 (2010) 337–341, https://doi.org/10.1126/science.1191968.
[34] B. Donzel, B. Kamber, K. Wüthrich, R. Schwyzer, A chiral cystine disulfide group without inherent optical activity in the long-wavelength region. (^{1}H- and ^{13}C-NMR., UV., CD., and ORD. Studies with cyclo-L-cystine), Helv. Chim. Acta 55 (1972) 947–961, https://doi.org/10.1002/hlca.19720550321.
[35] U. Ludescher, R. Schwyzer, On the chirality of the cystine disulfide group: assignment of helical sense in a model compound with a dihedral angle greater than ninety degrees using NMR and CD, Helv. Chim. Acta 54 (1971) 1637–1644, https://doi.org/10.1002/hlca.19710540615.
[36] R.W. Woody, Application of the Bergson model to the optical properties of chiral disulfides, Tetrahedron 29 (1973) 1273–1283, https://doi.org/10.1016/S0040-4020(01)83144-6.
[37] T. Kurtán, G. Pescitelli, P. Salvadori, Á. Kenéz, S. Antus, L. Szilágyi, T.-Z. Illyés, I. Szabó, Circular dichroism of diglycosyl dichalcogenides in solution and solid state, Chirality 20 (2008) 379–385, https://doi.org/10.1002/chir.20458.
[38] J.T. Vázquez, Features of electronic circular dichroism and tips for its use in determining absolute configuration, Tetrahedron: Asymmetry 28 (2017) 1199–1211, https://doi.org/10.1016/j.tetasy.2017.09.015.
[39] G. Pescitelli, ECD exciton chirality method today: a modern tool for determining absolute configurations, Chirality 34 (2022) 333–363, https://doi.org/10.1002/chir.23393.
[40] X.-H. Gu, Y. Lei, S. Wang, F. Cao, Q.i. Zhang, S. Chen, K.-P. Wang, Z.-Q. Hu, Tetrahydro[5]helicene fused nitrobenzoxadiazole as a fluorescence probe for hydrogen sulfide, cysteine/homocysteine and glutathione, Spectrochim. Acta A 229 (2020) 118003, https://doi.org/10.1016/j.saa.2019.118003.
[41] Y.-H. Chen, J.-C. Tsai, T.-H. Cheng, S.-S. Yuan, Y.-M. Wang, Sensitivity evaluation of NBD-SCN towards cysteine/homocysteine and its bioimaging applications, Biosens. Bioelectron. 56 (2014) 117–123, https://doi.org/10.1016/j.bios.2014.01.009.
[42] J. Wang, L. Niu, J. Huang, Z. Yan, J. Wang, A novel NBD-based fluorescent turn-on probe for the detection of cysteine and homocysteine in living cells, Spectrochim. Acta A 192 (2018) 52–58, https://doi.org/10.1016/j.saa.2017.10.064.
[43] W. Wang, M. Ji, J. Chen, P. Wang, A novel turn-on type AIE fluorescent probe for highly selective detection of cysteine/homocysteine and its application in living cells, Talanta 239 (2022) 123091, https://doi.org/10.1016/j.talanta.2021.123091.
[44] H. Zhang, W. Li, J. Chen, G. Li, X. Yue, L. Zhang, X. Song, W. Chen, Simultaneous detection of Cys/Hcy and H_2S through distinct fluorescence channels, Anal. Chim. Acta 1097 (2020) 238–244, https://doi.org/10.1016/j.aca.2019.11.029.
[45] X. Ren, Y. Zhang, F. Zhang, H. Zhong, J. Wang, X. Liu, Z. Yang, X. Song, Red-emitting fluorescent probe for discrimination of Cys/Hcy and GSH with a large stokes shift under a single-wavelength excitation, Anal. Chim. Acta 1097 (2020) 245–253, https://doi.org/10.1016/j.aca.2019.11.030.
[46] Y. Zhang, J. Wang, Y. Yue, J. Chao, F. Huo, C. Yin, A new strategy for the fluorescence discrimination of Cys/Hcy and GSH/H_2S simultaneously colorimetric detection for H_2S, Spectrochim. Acta A Mol. Biomol. Spectrosc. 227 (2020) 117537, https://doi.org/10.1016/j.saa.2019.117537.
[47] W. Chen, H. Luo, X. Liu, J.W. Foley, X. Song, Broadly applicable strategy for the fluorescence based detection and differentiation of glutathione and cysteine/homocysteine: demonstration in vitro and in vivo, Anal. Chem. 88 (2016) 3638–3646, https://doi.org/10.1021/acs.analchem.5b04333.
[48] S. Grimme, C. Bannwarth, P. Shushkov, A robust and accurate tight-binding quantum chemical method for structures, vibrational frequencies, and noncovalent interactions of large molecular systems parametrized for all Spd-block elements (Z= 1–86), J. Chem. Theory Comput. 13 (2017) 1989–2009, https://doi.org/10.1021/acs.jctc.7b00118.
[49] T. Lu, Molclus Program, Version 1.9.9.6, http://www.keinsci.com/research/molclus.html.
[50] M.J. Frisch, G.W. Trucks, H.B. Schlegel, G.E. Scuseria, M.A. Robb, J.R. Cheeseman, G. Scalmani, V. Barone, B. Mennucci, G.A. Petersson, H. Nakatsuji, M. Caricato, X. Li, H.P. Hratchian, A.F. Izmaylov, J. Bloino, G. Zheng, J.L. Sonnenberg, M. Hada, M. Ehara, K. Toyota, R. Fukuda, J. Hasegawa, M. Ishida, T. Nakajima, Y. Honda, O. Kitao, H. Nakai, T. Vreven, J.A. Montgomery, J.E. Peralta, F. Ogliaro, M. Bearpark, J.J. Heyd, E. Brothers, K.N. Kudin, V.N. Staroverov, R. Kobayashi, J. Normand, K. Raghavachari, A. Rendell, J.C. Burant, S.S. Iyengar, J. Tomasi, M. Cossi, N. Rega, J. M. Millam, M. Klene, J.E. Knox, J.B. Cross, V. Bakken, C. Adamo, J. Jaramillo, R. Gomperts, R.E. Stratmann, O. Yazyev, A.J. Austin, R. Cammi, C. Pomelli, J.W. Ochterski, R.L. Martin, K. Morokuma, V.G. Zakrzewski, G.A. Voth, P. Salvador, J.J. Dannenberg, S. Dapprich, A.D. Daniels, O. Farkas, J.B. Foresman, J.V. Ortiz, J. Cioslowski, D.J. Fox, Gaussian 16, Revision B.01, Gaussian, Inc., Wallingford CT, (2016). http://gaussian.com.
[51] T. Bruhn, A. SchaumLöffel, Y. Hemberger, G. Pecitelli, SpecDis version 1.71, Berlin, Germany, (2017). https://specdis-software.jimdo.com.
[52] M. Sasmal, A.S.M. Islam, R. Bhowmick, D. Maiti, A. Dutta, M. Ali, Site-selective interaction of human serum albumin with 4-chloro-7-nitro-1,2,3-benzoxadiazole modified olanzapine derivative and effect of β-cyclodextrin on binding: in the light of spectroscopy and molecular docking, ACS Appl. Bio Mater. 2 (2019) 3551–3561, https://doi.org/10.1021/acsabm.9b00429.
[53] S. Adhikari, J.S. Kang, W. Lee, A Convenient and validated enantiomer separation of chiral aliphatic amines as nitrobenzoxadiazole derivatives on polysaccharide-derived chiral stationary phases under simultaneous ultraviolet and fluorescence detection, Chirality 28 (2016) 789–794, https://doi.org/10.1002/chir.22659.
[54] E. Özdemir, G. Ergin Kizilçay, S. Ertürk Toker, Development and validation of two new methods for the determination of rilmenidine in bulk and pharmaceutical preparation, J. Chromatogr. Sci. (2021) 1-6. https://doi.org/10.1093/chromsci/bmab035.
[55] J. Yao, G. Yin, T. Yu, H. Li, P. Yin, Simultaneous sensing of cysteine/homocysteine and glutathione with a fluorescent probe based on a single atom replacement strategy, Anal. Methods 13 (2021) 1358–1363, https://doi.org/10.1039/d0ay02206c.
[56] C.S. Sevier, C.A. Kaiser, Formation and transfer of disulphide bonds in living cells, Nat. Rev. Mol. Cell Biol. 3 (2002) 836–847, https://doi.org/10.1038/nrm954.
[57] J.P. Casey, R.B. Martin, Disulfide stereochemistry. Conformations and chiroptical properties of L-cystine derivatives, J. Am. Chem. Soc. 94 (1972) 6141–6151, https://doi.org/10.1021/ja00772a036.
[58] V. Pattabha, R. Srinivasan, On the conformation of the disulphide group in L-cystine and its derivatives, Int. J. Pept. Protein Res. 8 (1976) 27–32, https://doi.org/10.1111/j.1399-3011.1976.tb02477.x.
[59] N. Harada, K. Nakanishi, N. Berova, Electronic CD Exciton Chirality Method: Principles and Applications in Comprehensive Chiroptical Spectroscopy: Applications in Stereochemical Analysis of Synthetic Compounds, Natural Products, and Biomolecules, N. Berova, P.L. Polavarapu, K. Nakanishi, R.W. Woody (Eds.), John Wiley & Sons: New York, NY, USA, (2012).
[60] G. Pescitelli, L. Di Bari, Exciton coupling between enones: quassinoids revisited, Chirality 29 (2017) 476–485, https://doi.org/10.1002/chir.22711.
[61] R.L. Martin, Natural transition orbitals, J. Chem. Phys. 118 (2003) 4775–4777, https://doi.org/10.1063/1.1558471.
[62] V.A. Spata, S. Matsika, Role of excitonic coupling and charge-transfer states in the absorption and CD spectra of adenine-based oligonucleotides investigated through QM/MM simulations, J. Phys. Chem. A 118 (2014) 12021–12030, https://doi.org/10.1021/jp507520c.

[63] A.Z. Johannes, R.K. Pingak, M. Bukit, Tauc plot software: calculating energy gap values of organic materials based on ultraviolet-visible absorbance spectrum, IOP Conf. Ser.: Mater. Sci. Eng. 823 (2020) 012030, https://doi.org/10.1088/1757-899X/823/1/012030.

[64] A.A.P. Khan, M. Nazim, A.M. Asiri, Efficient catalytic degradation of organic pollutants with cupric oxide nanomaterials in aqueous medium, J. Environ. Chem. Eng. 9 (2021) 106305, https://doi.org/10.1016/j.jece:2021.106305.

[65] S.N. Mthembu, A. Sharma, F. Albericio, B.G. de la Torre, Breaking a couple: disulfide reducing agents, ChemBioChem 21 (2020) 1947–1954, https://doi.org/10.1002/cbic.202000092.

[66] H.H. Jo, X. Gao, L. You, E.V. Anslyn, M.J. Krische, Application of a high-throughput enantiomeric excess optical assay involving a dynamic covalent assembly: parallel asymmetric allylation and Ee sensing of homoallylic alcohols, Chem. Sci. 6 (2015) 6747–6753, https://doi.org/10.1039/C5SC02416A.